The Adequacy of the Hydrostatic Assumption in Sea Breeze Modeling over Flat Terrain

CHARLES L. MARTIN

Simpson Weather Associates, Charlottesville, VA 22901

ROGER A. PIELKE

Department of Atmospheric Science, Colorado State University, Fort Collins, 80523

(Manuscript received 15 December 1982, in final form 11 March 1983)

ABSTRACT

Using a linear analytic model and a nonlinear numerical model, the adequacy of the hydrostatic model is investigated for use in the simulation of sea and land breezes over flat terrain. Among the results it is found that for a given horizontal scale of heating, the hydrostatic assumption becomes less valid as the intensity of surface heating increases, and as the synoptic temperature lapse rate becomes less stable. The spatial scale at which the hydrostatic assumption fails is substantially smaller than suggested by Orlanski (1981). For sufficiently stable large-scale thermodynamic stratifications, for instance, aspect ratios of order unity can still produce nearly identical solutions, regardless of whether or not the hydrostatic assumption is used. The difference in the conclusions between our study and that of Orlanski is attributed to Orlanski's analyses of the characteristic wave equations in the free atmosphere, whereas in a sea-breeze simulation the requirement that vertical velocity at the ground is zero limits the magnitude of the vertical acceleration.

1. Introduction

There has been considerable discussion regarding the adequacy of the hydrostatic assumption in mesoscale meteorological models; however, much of it has utilized scale analysis in order to estimate the magnitude of error introduced when the hydrostatic assumption is used. Such scale analyses are performed either on the vertical equation of motion alone, (*e.g.*, Pielke, 1981, Section 3; Haltiner and Williams, 1980; Neuman and Mahrer, 1971) or on a linearized set of the equations of motion (*e.g.*, Pielke, 1981, Section 5; Haltiner and Williams, 1980). Unfortunately, the use of scale analysis permits only a qualitative evaluation of the suitability of the hydrostatic assumption.

In order to more quantitatively determine the error introduced using this assumption, it is desirable to utilize models with and without this formulation for the vertical pressure distribution. Two models are used in this study—a linear model originally developed by Defant (1950) and a nonlinear analog to that model, described in Martin (1981). The analytic linear model provides the investigator with the ability to explore the significance of the hydrostatic assumption without the complication of computational errors, whereas the nonlinear model provides the opportunity to investigate the contribution of advection to errors introduced using the hydrostatic relation.

2. Basic equations

The basic equations used in this study are of the two-dimensional form used by Defant (1950). They are

$$\frac{\partial u'}{\partial t} = -\alpha_0 \frac{\partial p'}{\partial x} + fv' - \alpha_0\left(\frac{\partial}{\partial z}\alpha_0^{-1}\overline{w''u''} + \frac{\partial}{\partial x}\alpha_0^{-1}\overline{u''^2}\right), \quad (1)$$

$$\frac{\partial v'}{\partial t} = -fu' - \alpha_0\left(\frac{\partial}{\partial z}\alpha_0^{-1}\overline{w''v''} + \frac{\partial}{\partial x}\alpha_0^{-1}\overline{u''v''}\right), \quad (2)$$

$$\lambda\frac{\partial w'}{\partial t} = g\frac{\theta'}{\theta_0} - \alpha_0\frac{\partial p'}{\partial z} - \lambda\alpha_0\left(\frac{\partial}{\partial z}\alpha_0^{-1}\overline{w''^2} + \frac{\partial}{\partial x}\alpha_0^{-1}\overline{u''w''}\right), \quad (3)$$

$$\frac{\partial u'}{\partial x} + \frac{\partial w'}{\partial z} = 0, \quad (4)$$

$$\frac{\partial \theta'}{\partial t} = -w'\frac{\partial \theta_0}{\partial z} - \alpha_0\left(\frac{\partial}{\partial z}\alpha_0^{-1}\overline{w''\theta''} - \frac{\partial}{\partial x}\alpha_0^{-1}\overline{u''\theta''}\right), \quad (5)$$

where the prime and double prime indicate mesoscale perturbations from the synoptic state and subgrid-scale fluctuations, respectively. The synoptic state is indicated by the subscript zero. To simplify the anal-

ysis, horizontal gradients in the synoptic fields are assumed zero, as are variations in the north–south direction. In addition, the Coriolis term is neglected in the vertical equation of motion [see Pielke, (1981, p. 197) for the justification], the incompressible continuity equation is used, and the subgrid-scale fluxes are assumed horizontally homogeneous. The parameter λ is identically zero in a hydrostatic model, while λ is equal to unity in the nonhydrostatic version.

a. Linear solution

In Defant's (1950) original version, advection was ignored in order to permit an exact analytic solution. Also,

$$\left.\begin{aligned}
\alpha_0\left(\frac{\partial}{\partial x}\alpha_0^{-1}\overline{u''^2} + \frac{\partial}{\partial z}\alpha_0^{-1}\overline{u''w''}\right) &= \sigma_H u' \\
\alpha_0\left(\frac{\partial}{\partial x}\alpha_0^{-1}\overline{u''v''} + \frac{\partial}{\partial z}\alpha_0^{-1}\overline{v''w''}\right) &= \sigma_H v' \\
\alpha_0\left(\frac{\partial}{\partial x}\alpha_0^{-1}\overline{u''w''} + \frac{\partial}{\partial z}\alpha_0^{-1}\overline{w''^2}\right) &= \sigma_v w' \\
\alpha_0\left(\frac{\partial}{\partial z}\alpha_0^{-1}\overline{w''\theta''} + \frac{\partial}{\partial x}\alpha_0^{-1}\overline{u''\theta''}\right) &= K\left(\frac{\partial^2\theta'}{\partial x^2} + \frac{\partial^2\theta'}{\partial z^2}\right)
\end{aligned}\right\} \quad (6)$$

were assumed. The formulation used by Defant (1980) to represent the subgrid-scale fluxes of velocity are not standard today, but do permit an evaluation of the relative contribution of subgrid-scale fluxes.

To solve (1)–(5) without advection in the five unknowns (*i.e.*, u', v', w', p' and θ'), Defant recognized that u' and v' must be 90° out of phase with w', p' and θ', since the first two dependent variables are expressed in terms of derivatives of the others. Moreover, the solutions should be a function of height above the ground surface, rather than simply a periodic function, since the sea and land breeze does not extend upward indefinitely. Defant, therefore, assumed solutions of the form

$$\left.\begin{aligned}
w'(x, z, t) &= \tilde{w}(z)e^{i\omega t}\sin k_x x \\
p'(x, z, t) &= \tilde{p}(z)e^{i\omega t}\sin k_x x \\
\theta'(x, z, t) &= \tilde{\theta}(z)e^{i\omega t}\sin k_x x \\
u'(x, z, t) &= \tilde{u}(z)e^{i\omega t}\cos k_x x \\
v'(x, z, t) &= \tilde{v}(z)e^{i\omega t}\cos k_x x
\end{aligned}\right\}, \quad (7)$$

with the boundary conditions

$$w'(z = 0) = w'(z \to \infty) = \theta'(z \to \infty) = 0,$$
$$\theta'(z = 0) = Me^{i\omega t}\sin k_x x,$$

where M is the amplitude of the maximum mesoscale perturbation surface potential temperature. In general, $\tilde{w}$, $\tilde{p}$, $\tilde{\theta}$, $\tilde{u}$ and $\tilde{v}$ are complex valued variables. The wavenumber k_x is equal to 2π divided by the wavelength L_x of the assumed periodic function. In this model, $0.5L_x$ corresponds to the size of land in which the maximum heating occurs $0.25L_x$ inland from the coast. The frequency ω represents the temporal periodic variation in the system which for a sea–land breeze simulation, corresponds to the diurnal period.

The assumed solutions given by (7) are substituted into (1)–(5) which, after simplification, yields

$$\left.\begin{aligned}
i\omega\tilde{u} &= -k_x\alpha_0\tilde{p} + f\tilde{v} - \sigma_H\tilde{u} \\
i\omega\tilde{v} &= -f\tilde{u} - \sigma_H\tilde{v} \\
i\omega\lambda\tilde{w} &= -\lambda\sigma_v\tilde{w} - \alpha_0\frac{d\tilde{p}}{dz} + \gamma\tilde{\theta} \\
-l_x\tilde{u} + \frac{d\tilde{w}}{dz} &= 0 \\
i\omega\tilde{\theta} &= -\tilde{w}\beta - K\tilde{\theta}k_x^2 + K\frac{d^2\tilde{\theta}}{dz^2}
\end{aligned}\right\}. \quad (8)$$

These equations, with boundary conditions, are solved simultaneously for the dependent variables, $\tilde{u}$, $\tilde{v}$, $\tilde{w}$, $\tilde{\theta}$ and $\tilde{p}$, which are now only functions of z. The solution to this set of linear ordinary differential equations is discussed in detail in Martin (1981) and is given by

$$\tilde{\theta}(z) = Me^{-bz} + \frac{b^2 - s}{b^2 - a^2}M\{e^{az} - e^{-bz}\}, \quad (9)$$

$$\tilde{w}(z) = \frac{-rM}{b^2 - a^2}(e^{az} - e^{-bz}), \quad (10)$$

$$\tilde{u}(z) = -\frac{1}{k_x}\frac{rM}{b^2 - a^2}(ae^{az} + be^{-bz}), \quad (11)$$

$$\tilde{v}(z) = \frac{f}{i\omega + \sigma_H}\frac{1}{k_x}\frac{rM}{b^2 - a^2}(ae^{az} + be^{-bz}), \quad (12)$$

$$\tilde{p}(z) = \frac{1}{\alpha_0 k_x^2}\frac{(i\omega + \sigma_H)^2 + f^2}{(i\omega + \sigma_H)} \times \frac{rM}{b^2 - a^2}(ae^{az} + be^{-bz}), \quad (13)$$

where

$$\left.\begin{aligned}
\eta^2 &= k_x^2\frac{(i\omega + \sigma_H)\lambda(i\omega + \sigma_v)}{(i\omega + \sigma_H)^2 + f^2} \\
r &= -\frac{\gamma k_x^2(i\omega + \sigma_H)}{(i\omega + \sigma_H)^2 + f^2} \\
\epsilon &= \frac{\beta}{K}, \quad s = \frac{i\omega}{K} + k_x^2
\end{aligned}\right\}. \quad (14)$$

And a and b are determined from

$$a^2 = b^2 = \tfrac{1}{2}(\eta^2 + s) \pm \tfrac{1}{2}[(\eta^2 + s)^2 - 4(\eta^2 s - \epsilon r)]^{1/2}. \quad (15)$$

It follows that a and b are given by

$$\left.\begin{aligned} a &= \pm\sqrt{a^2} \\ b &= \pm\sqrt{b^2} \end{aligned}\right\} \quad (16)$$

The choice remains of which roots to choose in (15) and (16). In order to avoid division by zero, a^2 and b^2 must be opposite roots of (15). Solutions of the model equations, however, showed that identical results were obtained whether a^2 was the first root and b^2 the second root of (15) or vice versa. Furthermore, to satisfy the boundary condition $w\ (z \to \infty) = 0$, in conjunction with (10), b must have a positive real part and a must have a negative real part. This is no restriction since the square roots of a complex number will yield one with a positive real part and one with a negative real part.

With this information, the analytic solution to Defant's linear model is obtained. Values of the dependent variables w', p', θ', u' and v' as a function of x, z and t are determined by calculating the real parts of (7) and (9) through (13), using (15), (16) and (14) in order to determine the values of η^2, γ, s, ϵ, a^2, b^2, a and b.

Fig. 1 illustrates $\tilde{u}$ and $\tilde{w}$ at 6 h after simulated sunrise obtained using this linear model. The values of the parameters used in the model were

$$\left.\begin{aligned} &\beta = 1°\text{C}\,1\text{ km}^{-1};\ K = 10\text{ m}^2\text{ s}^{-1}; \\ &\alpha_0 = 0.758\text{ m}^3\text{ kg}^{-1} \\ &\sigma_H = \sigma_v = 10^{-3}\text{ s}^{-1};\ f = 1.031 \times 10^{-4}\text{ s}^{-1}; \\ &g = 9.8\text{ m s}^{-2} \\ &\theta_0 = 273\text{ K};\ M = 10°\text{C}; \\ &k_x = 2\pi\ 100\text{ km}^{-1} \end{aligned}\right\} \quad (17)$$

The symmetric circulation evident in the figure results because of the horizontal periodicity assumed in the solutions and the neglect of advective effects (see Sections 2b1, 2b2). Land and water are differentiated in the model only by the magnitude of k_x [the same dependent variables over water and land are always of opposite sign because of the form of the assumed solution (7)].

This solution illustrates the interrelation between the dependent variables. Because of the prescribed heating/cooling pattern in the model, pressure falls develop in the region of heating, while rises occur where cooling is specified. This pressure pattern causes horizontal accelerations toward regions of lower pressure, as required by (1). Since mass conservation is required from (4), upward motion necessarily results in the region of heating, while subsidence occurs in the areas of cooling.

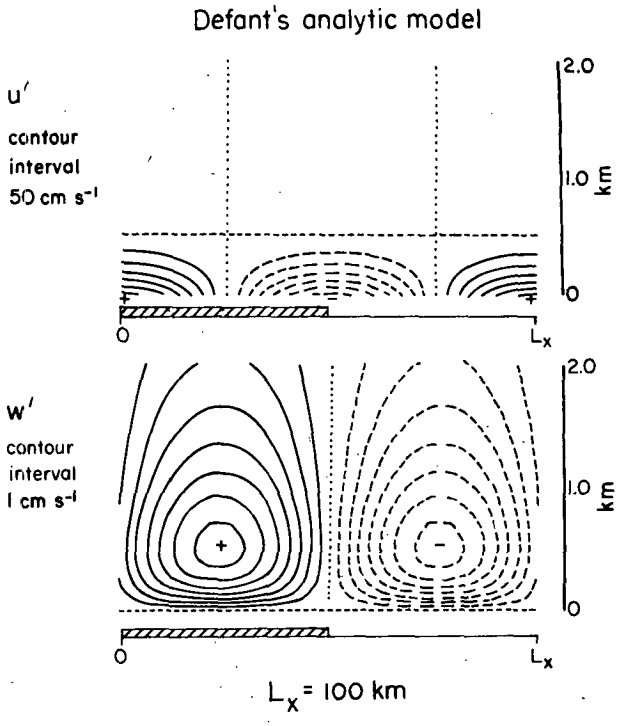

FIG. 1. The horizontal and vertical velocity fields predicted from Defant's (1950) model 6 h after sunrise using the input parameters given by (17). The zero in this and subsequent figures is indicated by the dotted line.

To examine the relative error between the non-hydrostatic and hydrostatic amplitudes of a given dependent variable, the quantity

$$E = 2\,\frac{|\phi_n| - |\phi_{nh}|}{|\phi_n| + |\phi_{nh}|} \quad (18)$$

is calculated, where $|\phi_n|$ and $|\phi_{nh}|$ are the maximum absolute amplitudes over time and space for a given set of parameters such as listed in (17). The subscripts n and nh correspond to hydrostatic and non-hydrostatic versions.

Fig. 2 illustrates one such comparison where E is evaluated as a function of the domain-averaged lapse rate $\partial\theta_0/\partial z$ and L_x. As the atmosphere becomes more stably stratified, according to Defant's model, the hydrostatic relation is a more accurate assumption for a given horizontal scale of the circulation.

With a value of $\partial\theta_0/\partial z = 1°\text{C}\ (100\text{ m})^{-1}$, for instance, the maximum error is less than 2% even with $L_x = 1$ km, whereas an equivalent level of accuracy is not attained for $\partial\theta_0/\partial z = 0.01°\text{C}\ (100\text{ m})^{-1}$ until $L_x \approx 10$ km. Fig. 3 shows a similar analysis for the magnitude of the exchange coefficient for heat, K, which is assumed a constant in a given solution of Defant's model. As the rate at which heat is mixed

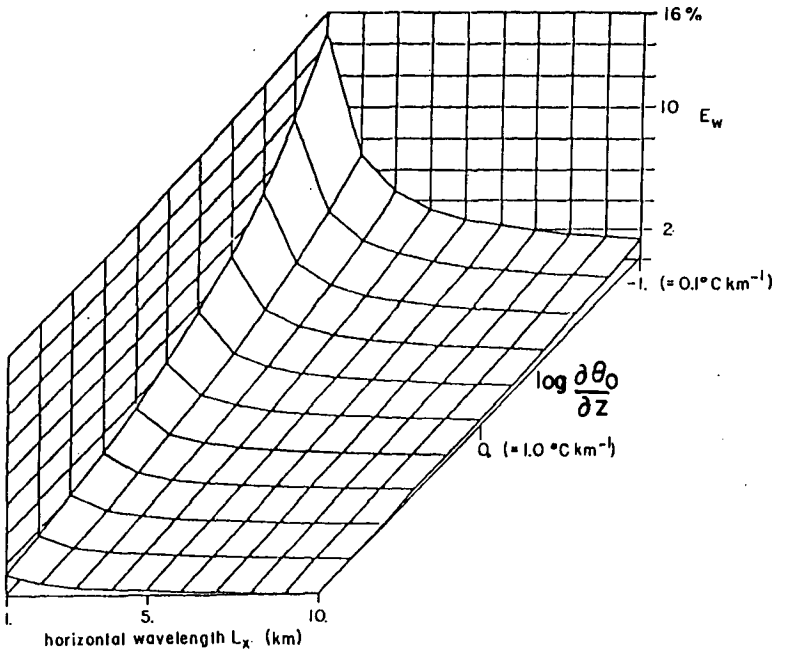

FIG. 2. Relative error in vertical velocity E_w, between non-hydrostatic and hydrostatic models. $\partial\theta_0/\partial z$ is in units of °C km^{-1}.

in the model increases, the hydrostatic relation becomes a poorer assumption for the pressure distribution in the model. With values of $K = 10^2$ m^2 s^{-1} and $L_x = 1$ km, for example, the maximum error is about 4%, while it increases to over 14% for $K = 10^3$ m^2 s^{-1}. [The sensitivity of the results to different values of σ_H and σ_v were also examined (Martin, 1981). For $\sigma_H = \sigma_v = 10^{-3}$ s^{-1}, for instance, the maximum

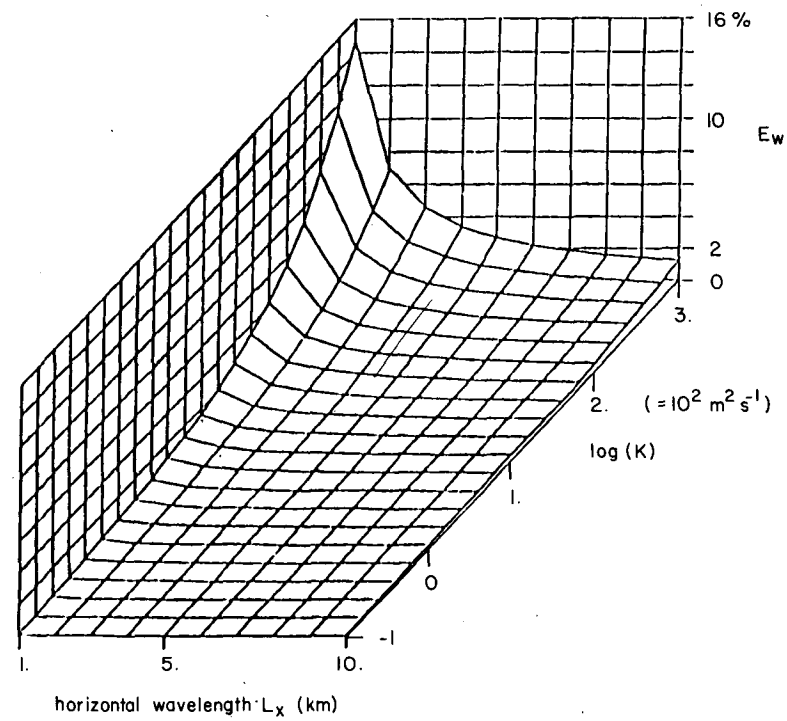

FIG. 3. Relative error in vertical velocity E_w between non-hydrostatic and hydrostatic models. K is in units of m^2 s^{-1}.

error introduced when the hydrostatic assumption was used was only 1% even for $L_x = 1$ km. Smaller values of σ_H and σ_v resulted in even smaller errors.]

These results are at variance to conclusions reached by Wipperman (1981) and Orlanski (1981). Wipperman suggested that the hydrostatic assumption is only valid for horizontal scales $\geq$ 10 km, while Orlanski claimed that $H_\rho/\Delta x \ll 1$ is needed before the hydrostatic assumption can be accurately applied. Both of these studies, however, examined only wave equations where no boundary conditions were applied. Thus, their conclusion regarding the hydrostatic assumption is only valid for meteorological systems where internal gravity wave propagation in the free atmosphere is the dominant disturbance. Consistent with the study discussed here, however, Wipperman found the hydrostatic assumption to be valid for smaller scales when the atmosphere is more stable. He also stated that increased wind speed has the same effect as decreased thermal stability.

b. *Nonlinear model*

A nonlinear model can be used to investigate the influence of advection on the adequacy of the hydrostatic assumption. In contrast to the linear solution, the horizontal scale of heating is not, in general, equal to the horizontal scale of the resultant mesoscale circulation.

The form of equations used in the nonlinear numerical model are given in Table 1 and are derived from (1)–(5) with the addition of advection in the prognostic equations. To approximate the individual terms, forward time differencing is used with centered in space differencing for the remaining terms, with the exception of the advection terms where upstream spline interpolation (*e.g.*, see Mahrer and Pielke, 1978) is used.

The nonhydrostatic model was derived, as originally suggested by Pielke (1973), by first differentiating (1) with respect to x, and (3) for $\lambda = 1$ with respect to z, and adding using (4) to eliminate the time tendency terms. After rearranging, a Poisson equation for the perturbation pressure is obtained. Traditionally, that equation is used to calculate pressure in a numerical nonhydrostatic model. An alternative formulation, however, is to differentiate (1) with respect to x, and (3) for $\lambda = 0$ with respect to z and adding. The result is a Poisson equation for the *hydrostatic pressure*. Subtracting the Poisson equation for the hydrostatic pressure from the Poisson equation for the total pressure yields a Poisson equation for the nonhydrostatic residual R (*i.e.*, $R = p' - p'_H$ where p' is the perturbation pressure and p'_H is the hydrostatic component of the perturbation pressure). The hydrostatic component is calculated from (3) with $\lambda = 0$, straightforwardly, using vertical integration. The Poisson equation for R is given in Table 1.

TABLE 1. Hydrostatic and nonhydrostatic nonlinear analogs to Defant's (1950) model.

Nonlinear analog to the Defant (1950) model	
Hydrostatic	Nonhydrostatic
(1) $\dfrac{\partial u'}{\partial t} = -u'\dfrac{\partial u'}{\partial x} - w'\dfrac{\partial u'}{\partial z'} - \alpha_0\dfrac{\partial p'_H}{\partial x} + fv' - \sigma_H u'$	(1) $\dfrac{\partial u'}{\partial t} = -u'\dfrac{\partial u'}{\partial x'} - w'\dfrac{\partial u'}{\partial z} - \alpha_0\dfrac{\partial p'}{\partial x} + fv' - \sigma_H u'$
(2) $\dfrac{\partial v'}{\partial t} = -u'\dfrac{\partial v'}{\partial x} - w'\dfrac{\partial v'}{\partial z} - fu' - \sigma_H v'$	(2) $\dfrac{\partial v'}{\partial t} = -u'\dfrac{\partial v'}{\partial x} - w'\dfrac{\partial v'}{\partial z} - fu' - \sigma_H v'$
(3) $\dfrac{\partial p'_H}{\partial z} = \dfrac{\theta'}{\theta_0\alpha_0} g$	(3) $\nabla^2 R = \dfrac{\partial^2}{\partial x^2}(p' - p'_H) + \dfrac{\partial^2}{\partial z^2}(p' - p'_H) = \dfrac{1}{\alpha_0}\left\{\dfrac{\partial}{\partial x}\dfrac{\partial u}{\partial t}\right\|^* - \dfrac{\partial}{\partial z}u'\dfrac{\partial w'}{\partial x} - \dfrac{\partial}{\partial z}w'\dfrac{\partial w'}{\partial z} - \sigma_v\dfrac{\partial w'}{\partial z}\Big\}$ (i)
	$\dfrac{\partial p'_H}{\partial z} = \dfrac{\theta'}{\theta_0\alpha_0} g$ (ii)
	$\dfrac{\partial u}{\partial t}\Big\|^* = -u'\dfrac{\partial u'}{\partial x'} - w'\dfrac{\partial u'}{\partial z} - \alpha_0\dfrac{\partial p'_H}{\partial x} + fv' - \sigma_H u'$ (iii)
	$p' = R + p'_H$ (iv)
(4) $\dfrac{\partial u'}{\partial x} + \dfrac{\partial w'}{\partial z} = 0$	(4) $\dfrac{\partial u'}{\partial x} + \dfrac{\partial w'}{\partial z} = 0$
(5) $\dfrac{\partial \theta'}{\partial t} = -u'\dfrac{\partial \theta'}{\partial x} - w'\dfrac{\partial \theta'}{\partial z} - w'\dfrac{\partial \theta_0}{\partial z} + K\left\{\dfrac{\partial^2\theta'}{\partial x^2} + \dfrac{\partial^2\theta'}{\partial z^2}\right\}$	(5) $\dfrac{\partial \theta'}{\partial t} = -u'\dfrac{\partial \theta'}{\partial x} - w'\dfrac{\partial \theta'}{\partial z} - w'\dfrac{\partial \theta_0}{\partial z} + K\left\{\dfrac{\partial^2\theta'}{\partial x^2} + \dfrac{\partial^2\theta'}{\partial z^2}\right\}$

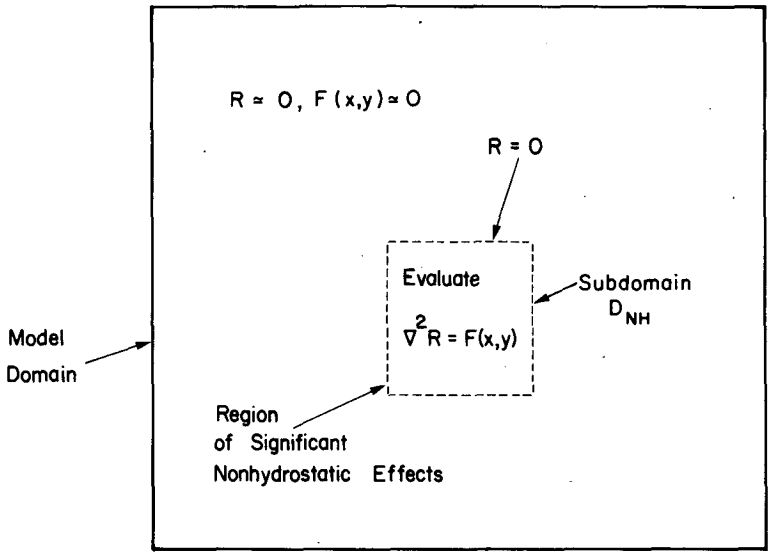

FIG. 4. Computation of a local nonhydrostatic effect in a numerical model.

One advantage of using such a formulation for R is that the Poisson equation need only be computed locally within a model domain outside of which $F(x, z)$ is arbitrarily small, as illustrated schematically in Fig. 4. The boundary conditions are also specified easily (*i.e.*, $R = 0$).

To check the numerical model code, an experiment was performed which used equivalent initial and boundary conditions [*i.e.*, as given by (17)] as applied to create Fig. 1. To be consistent, all the advection terms were removed in the calculations. The numerical results, shown in Fig. 5, correspond closely with the analytic results (Fig. 1), indicating that the computational code has been formulated consistent with Defant's model.

Before illustrating comparisons of hydrostatic and nonhydrostatic results for different horizontal scales of heating, several other aspects of the model results will be discussed in order to examine the influence of the assumed lower boundary condition on the spatial scales of the solution. In these experiments a relatively large value of L_x was chosen in order to assure that the hydrostatic assumption is valid.

1) EFFECT OF SURFACE HEATING

Fig. 6 illustrates two numerical experiments performed using the initial parameters given by (17), except $M = 1$°C in the first simulation. Since the spatial pattern of the linear solution is identical regardless of the magnitude of the amplitude M of surface heating, Defant's model predicts a solution of the form illustrated by Fig. 1, for both $M = 1$°C and $M = 10$°C. From (9)–(13), the magnitude of the perturbations are only multiplied by M, but with no alteration in the vertical or horizontal scale of the circulation.

The nonlinear results, in contrast, show a marked difference between $M = 1$ and 10°C. For the smaller magnitude of heating, the linear and nonlinear results are almost identical. For $M = 10$°C, however, the horizontal scale of the low-level convergence is much smaller and of the low-level divergence larger than expected from the linear solution. Such asymmetry develops because the advection enhances the convergence of the region of heating, thereby causing a larger horizontal pressure gradient. This increased pressure gradient generates additional convergence

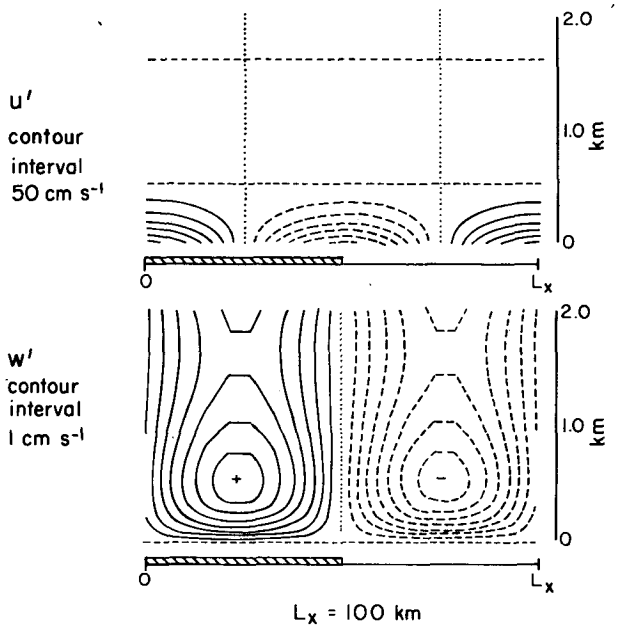

FIG. 5. The numerical analog to Defant's (1950) model using input as in Fig. 1.

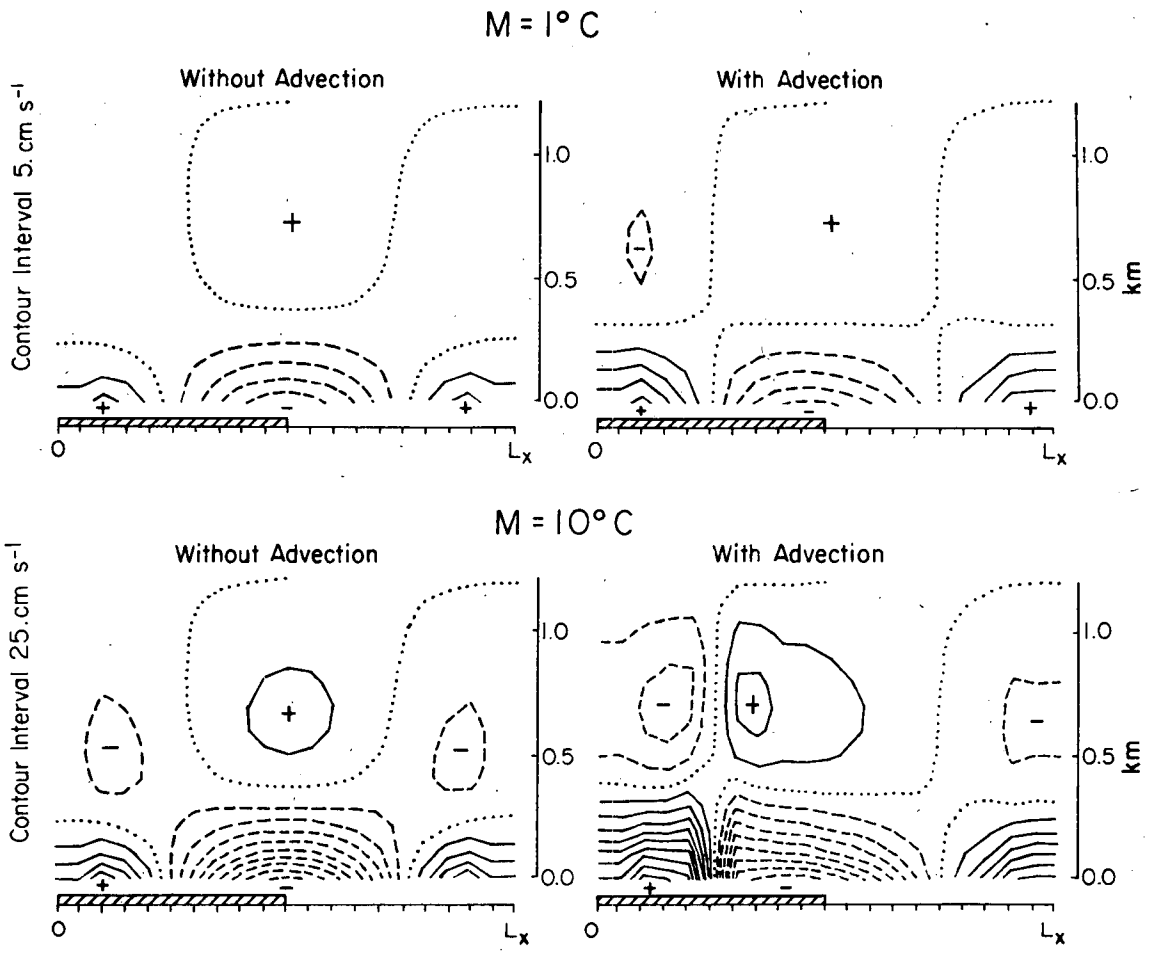

FIG. 6. The simulation of the sea breeze using the numerical analog of Defant's model with M = 1°C (top) and 10°C (bottom), without (left) and with nonlinear advection included.

due to horizontal advection, and this *positive feedback* continues until frictional retardation or the cooling of the surface limits the horizontal velocity acceleration.

With regard to the hydrostatic assumption, however, the reduction in horizontal scale due to nonlinear advection, indicates that a nonlinear model must be used in order to examine the importance of nonhydrostatic pressure forces when advection is significant.

2) EFFECT OF SPATIAL DISTRIBUTION OF THE SURFACE HEATING

Fig. 7 (left) was created assuming a sinusoidal form of surface heating [*i.e.*, as given following (7)] with nonlinear advection included. Fig. 7 (right) illustrates results when the same magnitude of heating is used (*i.e.*, M = 2.5°C) with L_x = 50 km, but the spatial temperature perturbation is assumed uniform over land and identically zero over water. Such a specification corresponds more closely with reality.

As compared with Fig. 7 (left), the low-level convergence is broader and less intense than when the sinusoidal form of surface heating is used. The result is that the horizontal scale of the horizontal circulation is larger than would be expected if the heating were sinusoidal. Perhaps the major reasons for the difference are that with sinusoidal heating: 1) horizontal accelerations are produced from both the left and the right of the location of maximum heating; and 2) the temperature decrease at the water surface when the spatial periodic function is used creates a maximum of 20°C, rather than 10°C difference between the land and water.

3) EFFECT OF THE HYDROSTATIC ASSUMPTION

In order to illustrate the effect of the hydrostatic assumption, it was elected to perform calculations using the sinusoidal heating function. Although less realistic than uniform heating over land, it should provide a minimum lower bound on the use of the hydrostatic assumption since the spatial scale of the

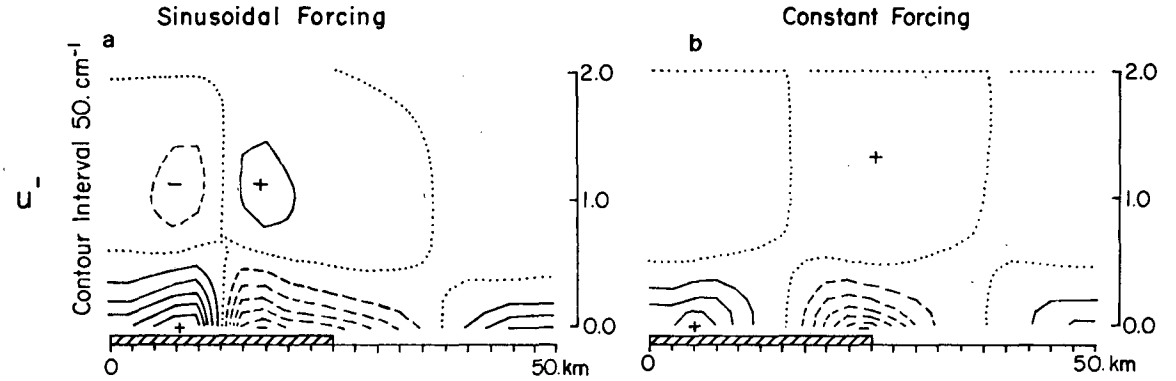

FIG. 7. The simulation of the sea breeze using the numerical analog of Defant's model with nonlinear advection for (a) sinusoidal surface heating function of the form given following (7); and (b) for a spatially constant value over land [*i.e.*, $\theta'(z = 0) = Me^{i\omega t}$ over land; zero otherwise].

circulation is expected to be smallest for this situation. It also permits a direct comparison with the analytic results discussed in Section 2a.

Figs. 8 and 9 illustrate two simulations with $L_x = 6.25$ km and with $L_x = 3.125$ km. The initial and boundary conditions are identical [and correspond to those given by (17)] except $M = 2.5°C$ and the period of the heating is 3 h for the $L_x = 6.25$ km simulation, and 1.5 h for the $L_x = 3.125$ calculation. Although this shortening of the time of heating was necessitated by limitations in available computer resources, it would be expected to enhance the nonhydrostatic effect. Thus, if the hydrostatic and nonhydrostatic results closely agree for these simulations, they would be even more closely in agreement for heating over a diurnal period.

As evident in the figures for the time of maximum heating over land, the results do closely correspond. The maximum differences between hydrostatic and nonhydrostatic simulations for the same scale of horizontal heating are:

	$L_x = 6.25$ km	$L_x = 3.125$ km
Max E_u	5.8%	5.7%
E_v	1.6%	3.0%
E_w	16.0%	18.0%
E_θ	0.8%	4.7%
E_p	10.0%	40.0%
Δu	31 cm s^{-1}	28 cm s^{-1}
Δv	0.3 cm s^{-1}	1.5 cm s^{-1}
Δw	15 cm s^{-1}	35 cm s^{-1}
$\Delta\theta$	0.006°C	0.011°C
Δp	0.022 mb	0.040 mb.

Here $\Delta A = ||A_{NH}|_{max} - |A_N|_{max}|$, with A representing any one of the dependent variables. The subscript max indicates that these are the largest calculated values for the entire simulation. E is the same as used in Figs. 2 and 3, and is defined by definition 18.

The relative contribution to a sea-breeze circulation of the nonhydrostatic pressure residual R is shown schematically in Fig. 10. Although of relatively

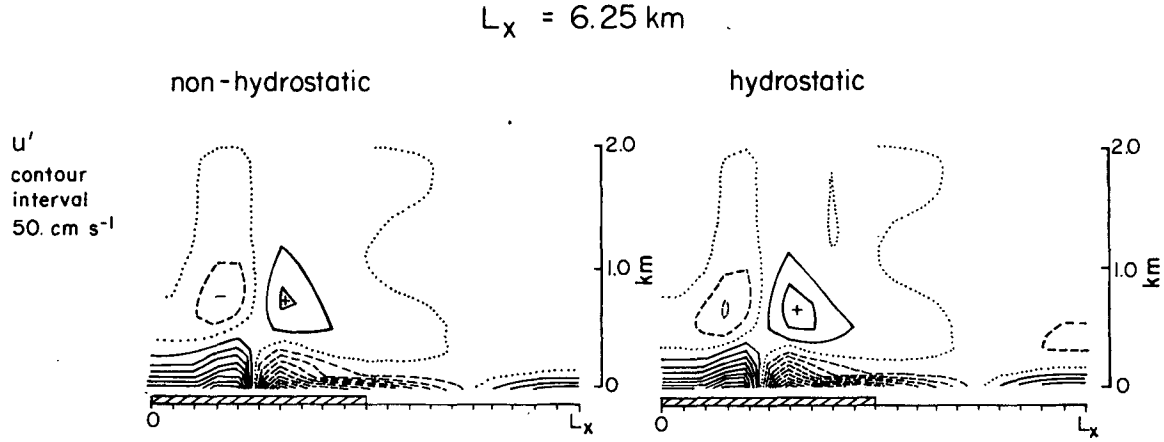

FIG. 8. Nonhydrostatic and hydrostatic simulations using the same initial and boundary conditions as given in (17), except $L_x = 6.25$ km, $\omega = 2\pi/3$ h and $M = 2.5°C$.

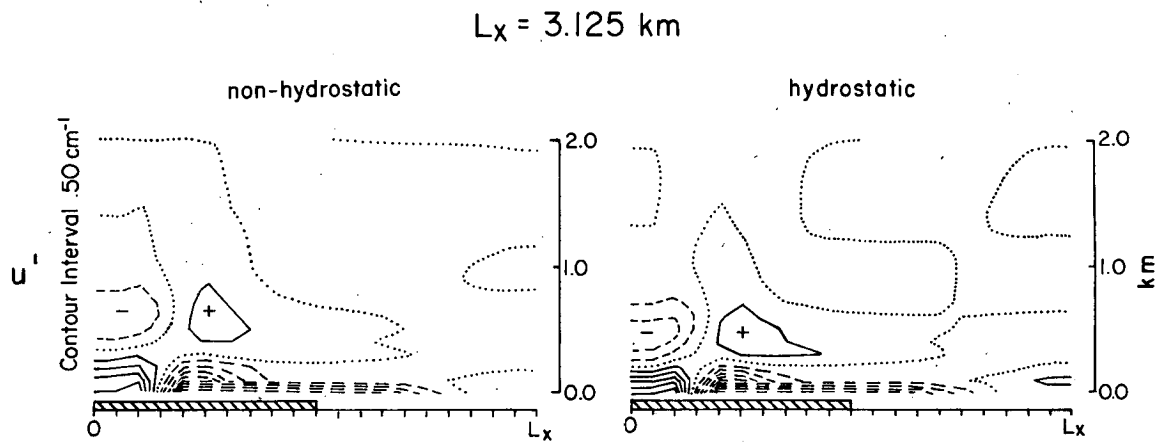

FIG. 9. As in Fig. 8, except L_x = 3.125 km and $\omega = 2\pi/1.5$ h.

small amplitude in the simulations shown in Figs. 8 and 9, the influence of R is to reduce the magnitude of the sea breeze disturbance, relative to the hydrostatic simulation. The value of R, as illustrated in Pielke (1972), is largest in the sea-breeze convergence zone.

Since the maximum differences in the vertical velocity results for the nonlinear simulation with L_x = 3.125 km and 6.25 km are 18 and 16%, it is clear that the reduction of the horizontal scale of the sea-breeze response reduces the applicability of the hydrostatic assumption. From the linear model solutions for the same initial and boundary conditions used to create Figs. 8 and 9, the differences in vertical velocity at the time of maximum heating between the hydrostatic and nonhydrostatic calculations are only 1 and 0.1%, respectively.

Therefore, for the initial and boundary conditions used here, the simulation with L_x = 6.25 km can justifiably be performed using a hydrostatic model. Even the case with L_x = 3.125 km deviates relatively little from the hydrostatic result indicating that for many applications a hydrostatic model can be used even for that horizontal scale of heating. This conclusion is consistent with the linear result and demonstrates that despite the reduction of the horizontal scale of the forcing by advection, the hydrostatic assumption can be used for spatial scales which are much smaller than suggested by Orlanski (1981). In fact, since the vertical and horizontal scales of the resultant circulation (estimated from the fields of u' in Figs. 8 and 9) are ~1.6 and 1.9 km for the L_x = 6.25 km simulation, and ~1.2 and 0.9 km for the 3.125 km case, even with aspect ratios near unity the results with and without the hydrostatic assumption are very similar.

The reason for the difference between our results and those of Orlanski, as suggested in Section 2a, is that Orlanski examined the solution of the wave equation in the free atmosphere, whereas here a mesoscale simulation forced by surface conditions was used. Since $w' \equiv 0$ at the ground is required, vertical accelerations must necessarily be reduced to a greater extent near the surface than would be expected at a higher level. This permits the hydrostatic assumption to be used with forcing of a smaller horizontal extent.

Orlanski (1981) was concentrating his discussion on a circulation in which conditional instability was realized through vertical lifting and saturation. Martin (1981) performed preliminary experiments in order to examine the influence of superadiabatic layers above the surface on the hydrostatic assumption. Although more work needs to be done in this area, the results reported in that study suggest that the hy-

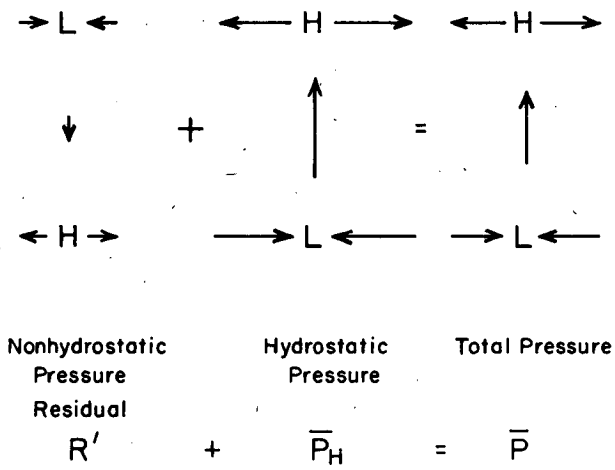

FIG. 10. A schematic of the relative contributions of the nonhydrostatic pressure residual and the hydrostatic pressure to the total pressure at a location over land in the center of the lowest surface pressure in the sea breeze convergence zone. The arrows illustrate the instantaneous horizontal ageostrophic winds that would be expected from this nonhydrostatic and hydrostatic pressure distribution. The nonhydrostatic pressure has its largest negative value at about the level of the largest upward vertical velocity in the sea breeze convergence zone. Adapted from Pielke (1972).

drostatic assumption may be less valid for the same spatial scale of heating when it is applied aloft, as when it occurs at the ground surface. This would be consistent with Orlanski's results which are straightforwardly applicable only to the free atmosphere.

3. Summary and conclusions

Using a linear and a nonlinear model, the adequacy of the hydrostatic assumption has been examined for use in sea- and land-breeze models over flat terrain. Although for significant surface heating, advection reduces the horizontal scale of the low-level circulation from that of the forcing, the results suggest that the hydrostatic assumption is valid to scales of heating and cooling at least as small as 6 km in sea- and land-breeze models over flat terrain. Since four grid increments (and preferably more) are needed to properly resolve a circulation in a numerical model, (*e.g.*, see Pielke, 1981), grid increments of 1.5 km or smaller may be appropriate in atmospheric models even if the hydrostatic assumption is used. Although this result appears to be contradictory to that found by Orlanski (1981), his result applies to free atmosphere wave motions and is intended to apply to situations where saturation in a conditionally unstable atmosphere creates large vertical acceleration. In a sea–land breeze simulation over flat terrain, the magnitude of the accelerations are limited by the requirement that the vertical velocity is identically zero at the ground.

Acknowledgments. This work was supported by the Atmospheric Science Section of the National Science Foundation under Grant #81073202 and was based on the M.S. thesis of the first author. Ray Arritt is thanked for performing several calculations during the preparation of the final draft. The drafting was performed by Judy Sorbie, while the typing was competently completed by Sara Rumley at Colorado State University.

REFERENCES

Defant, F., 1950: Theorie der land- und seewind. *Arch. Meteor. Geophys. Bioklim.*, **2**, 404–425.

Haltiner, G. J., and R. T. Williams, 1980: *Numerical Prediction and Dynamic Meteorology*, 2nd ed. Wiley.

Mahrer, Y., and R. A. Pielke, 1978: A test of an upstream spine interpolation technique for the advective terms in a numerical mesoscale model. *Mon. Wea. Rev.*, **106**, 818–830.

Martin, C. L., 1981: Numerical accuracy in a mesoscale meteorological model. M.S. thesis, University of Virginia, Charlottesville, 86 pp. [Available from the Sci. Tech. Library, University of Virginia 22903.]

Neumann, J., and Y. Mahrer, 1971: A theoretical study of the land and sea breeze circulation. *J. Atmos. Sci.*, **28**, 532–542.

Orlanski, I., 1981: The quasi-hydrostatic approximation. *J. Atmos. Sci.*, **38**, 572–582.

Pielke, R. A., 1973: Comparison of a hydrostatic and an analastic dry shallow primitive equation model. NOAA Tech. Memo. ERL OD-13, 47 pp. [Available from ERL-NOAA, Boulder, CO 80302.]

——, 1981: Mesoscale numerical modeling. *Advances in Geophysics*, Vol. 23, Academic Press, 185–344.

Wipperman, F., 1981: The applicability of several approximations in meso-scale modelling—A linear approach. *Contrib. Atmos. Phys.*, **54**, 298–308.